

# Room temperature Silicon detector for IR range coated with Ag<sub>2</sub>S Quantum Dots

*Ivan Tretyakov<sup>1\*</sup>, Alexander Shurakov<sup>1</sup>, Sergey Ryabchun<sup>1,2</sup>, Alexey Perepelitsa<sup>1,3</sup>, Natalya Kaurova<sup>1</sup>, Tatyana Zilberley<sup>4</sup>, Dmitry Zhukalin<sup>3</sup> and Gregory Goltsman<sup>1,2</sup>*

<sup>1</sup> Moscow State University of Education, Moscow 119435, Russia.

<sup>2</sup> National Research University Higher School of Economics, Moscow 101000, Russia.

<sup>3</sup> Voronezh State University, Voronezh 394018, Russia.

<sup>4</sup> Moscow Institute of Physics and Technology (State University), Dolgoprudny 141701, Russia.

**E-mail:** ivantretykov@mail.ru

**Keywords:** infrared range, silicon, quantum dot, surface states, room-temperature detector.

**Abstract:** For decades silicon has been the chief technological semiconducting material of modern microelectronics and has had a strong influence on almost all aspects of society. Applications of Si-based optoelectronic devices are limited to the visible and near infrared ranges. For photons with energy less than 1.12 eV silicon is almost transparent. The expansion of the Si absorption band to shorter wavelengths of the infrared range is of considerable interest to optoelectronic applications. By creating impurity states in Si it is possible to cause sub-band gap photon absorption. Here, we present an elegant and effective technology of extending the photoresponse of towards the IR range. Our approach is based on the use of Ag<sub>2</sub>S quantum dots (QDs) planted on the surface of Si to create impurity states in Si band gap. The specific sensitivity of the room temperature zero-bias Si\_Ag<sub>2</sub>S detector is  $10^{11}$  cm<sup>2</sup>/HzW<sup>-1</sup> at 1.55μm. Given the variety of available QDs and the ease of extending the photoresponse of Si towards the IR range, our findings open a path towards the future study and development of Si detectors for technological applications. The current research at the interface of

physics and chemistry is also of fundamental importance to the development of Si optoelectronics of the IR range.

The detection of low power radiation of the IR range presents great challenges to Si-based optoelectronics. The development of effective room-temperature photoconductors for the IR compatible with the current silicon technology is in great demand. In particular, megapixel digital imaging based on complementary-metal-oxide-semiconductor (CMOS) technology in the IR range has a high potential for crucial technological applications such as night vision systems, spectroscopy, medical diagnosis, environmental monitoring, on-chip optical data processing and astronomy.<sup>[1-6]</sup>

At room temperature Si has an indirect band gap  $\Delta E$  of 1.12 eV, for this reason Si is transparent for IR radiation from a wavelength of 1.1  $\mu\text{m}$ . This significantly limits the range of applications of current Si photoconductive devices. Various methods have been proposed to extend the photo-response of Si towards longer wavelengths of the IR range. One of them uses "heavy" doping of Si with chalcogen atoms Se and transition metals (Au, Ag, Ti, etc.).<sup>[7-11]</sup> Such hyperdoped materials offer an absorption coefficient increased by a factor of 2.5 in the IR range. Another approach is to integrate non-silicon electro-optical materials, such as direct-band gap III–V compound semiconductors (GaAs, InAs) with excellent IR photo-response. However, this way is strongly limited by the lattice mismatch between Si and these materials.<sup>[12]</sup> 2D materials do not suffer from this limitation and can be transferred to any substrate and used for IR and THz detection.<sup>[13-16]</sup> CVD-grown graphene monolayer coated with PbS QDs was monolithically integrated with silicon-integrated circuits based on CMOS for digital imaging in the IR range.<sup>[17]</sup>

In this paper, we report on the significant room-temperature photo-response of a Si photo-detector in the near-IR (NIR) and short-wave IR (SWIR). The sensibilization is possible by doping the Si surface by individual semiconducting  $\text{Ag}_2\text{S}$  QDs. This results in the formation of impurity states in the band gap of Si, which leads to the significant enhancement of the sub-band

gap photo-response. Additionally, it enables room-temperature operation of our detector, since Ag<sub>2</sub>S QDs introduce relatively high acceptor levels in the Si band gap, which mitigate thermal carrier generation.

Semiconducting QDs are nanocrystals with a size of the order of the Bohr radius of the Wannier-Mott exciton in the corresponding material.<sup>[18]</sup> Using QDs of different composition allows adjusting the spectral range of the detector depending on the absorption region of the QD.<sup>[19-22]</sup> Interest in using QDs is also due to the ease of the adjustment of the optical properties of the QD by changing its size.<sup>[23-25]</sup> Ag<sub>2</sub>S has a relatively narrow band gap of 1.0 eV in bulk and a high concentration of trap states, the presence of which is associated with QD nonstoichiometry.<sup>[26-29]</sup> The aqueous solutions of AgNO<sub>3</sub> and Na<sub>2</sub>S were used as the initial reagents aqueous synthesis of colloidal Ag<sub>2</sub>S QDs was carried out under conditions similar to described in Ref. 30 and Ref. 31. In order to remove the reaction by-products the acetone was used in aqueous colloidal Ag<sub>2</sub>S QDs solution followed by centrifuging the solution. Thioglycolic acid molecules were used as stabilizers.

Initial Si structures were fabricated using standard methods of laser lithography, thermal metal deposition and a lift-off process based on undoped high-resistance Si ( $\rho > 3 \text{ K}\Omega\cdot\text{cm}$ ). Using laser lithography, the width of the Ti/Au contacts  $W$  and the distance between them  $L$  were defined, thereby determining the geometric dimensions of the original Si structure,  $W$  and  $L$  were equal to 10  $\mu\text{m}$ . The contacts to the Si structure were formed by sequential thermal deposition of Ti and Au. **Figure 1a** shows an optical image and design of the investigated devices. During the fabrication process of Si-Ag<sub>2</sub>S devices, the quality and purity of the Si surface between the Ti/Au contacts is important. Before depositing colloidal Ag<sub>2</sub>S from the solution on top of Si, its surface was cleaned by ion etching in an Ar and O<sub>2</sub> atmosphere and liquid etching with hydrofluoric acid. The cleaning processes made it possible to remove of all impurities and natural oxides on the Si surface. Ag<sub>2</sub>S QDs from a colloidal solution were centrifuged onto a prepared Si surface between the Ti/Au contacts with the subsequent evaporation of the solvent. **Figure 1b** shows the Si surface between the Ti/Au contacts obtained by TEM after deposition of Ag<sub>2</sub>S QDs. Structural properties of the

devices were obtained using microscopy and X-ray diffraction analysis. The analysis of the TEM images shows that QDs are formed with average sizes of  $2.5 \pm 0.5$  nm. High resolution TEM images show the diffraction on the (012) atomic plane of monoclinic  $\text{Ag}_2\text{S}$  lattice. This fact indicates the formation of crystalline  $\text{Ag}_2\text{S}$  nanoparticles. The X-ray diffraction data also confirm the formation of  $\text{Ag}_2\text{S}$  nanocrystals with a monoclinic lattice (space group P 21/c). X-ray reflections were broadened due to the size effect. As can be seen from **Figure 1b**,  $\text{Ag}_2\text{S}$  QDs located on the Si surface don't interact with each other.

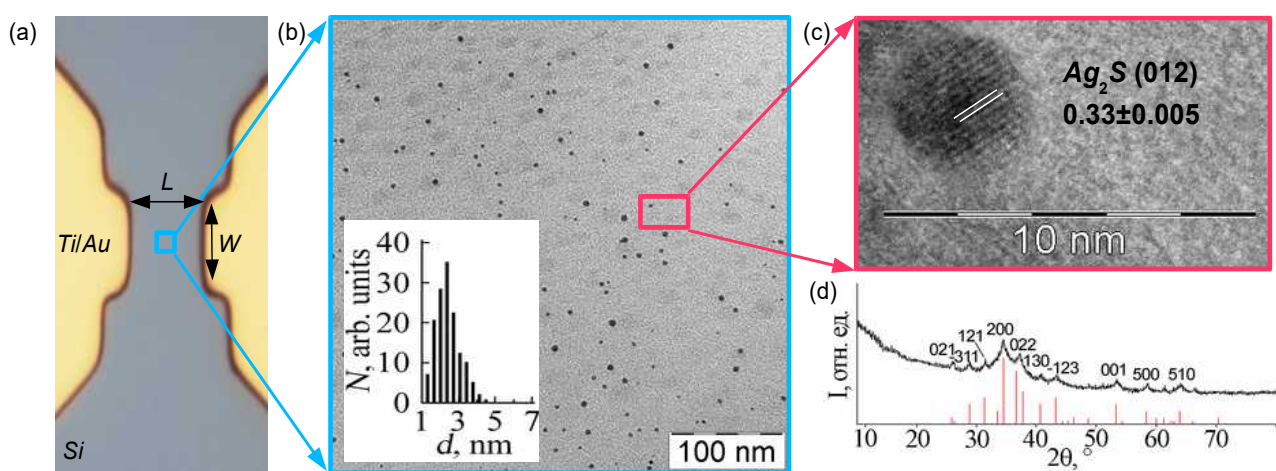


**Figure 1.** a) An optical image of the devices; IR radiation was focused on Si surface between Ti/Au. b) A TEM image of the Si surface after the deposition of  $\text{Ag}_2\text{S}$  QDs; the QDs were formed with average sizes of  $2.5 \pm 0.5$  nm and didn't come into contact with each other. c) A high-resolution TEM image of  $\text{Ag}_2\text{S}$  QDs on top of Si. The diffraction on the (012) atomic plane of the monoclinic  $\text{Ag}_2\text{S}$  lattice indicates the formation of crystalline  $\text{Ag}_2\text{S}$  nanoparticles; d) X-ray diffraction data for  $\text{Ag}_2\text{S}$  nanocrystals with a monoclinic lattice.

The extension of the spectral response and sensitivity for  $\text{Ag}_2\text{S}$ \_Si devices in the NIR and SWIR ranges were studied experimentally. The devices were shielded from the background radiation and in the absence of IR radiation had a resistance R of 20 MΩ. To couple the devices with IR radiation we used a hyper-hemispherical Si lens. The IR radiation incident on the lens was

collected into an Airy spot on the Si surface between the Ti/Au contacts. The studies of the spectral response  $S_v(\lambda)$  of our devices were performed in the range of 1 - 2  $\mu\text{m}$ , at 300K and zero bias device mode. **Figure 2** presents  $S_v(\lambda)$  for Si and Si\_Ag<sub>2</sub>S devices. The  $S_v(\lambda)$  dependence for Si device is given for bright estimation of the IR band extension for the Si\_Ag<sub>2</sub>S device. The  $S_v(\lambda)$  dependence of the Si device in **Figure 2** has a maximum at 1.1  $\mu\text{m}$  and drops rapidly already at 1.25  $\mu\text{m}$ . At same time,  $S_v(\lambda)$  for the Si\_Ag<sub>2</sub>S device demonstrates a monotonic fall down to 2  $\mu\text{m}$ . The cut-off wavelength of the internal photovoltaic effect for bulk Ag<sub>2</sub>S is around 1.25  $\mu\text{m}$ . Considering this fact, the strong response of the Si\_Ag<sub>2</sub>S device above 1.25  $\mu\text{m}$  can be explained by the formation of "surface states" caused by the Ag<sub>2</sub>S QDs coating on the Si surface. In the Si\_Ag<sub>2</sub>S device, when an IR photon is absorbed by an electron in the valence band of Si, the generated carrier transits at sub-band states Ag<sub>2</sub>S. This process is detected as a voltage change between the Ti/Au device contacts. For a quantitative evaluation of the Si sensitization effect, it is convenient to bring the ratio of the signal for the Si\_Ag<sub>2</sub>S structure to the signal for the Si structure taken at a given  $\lambda$ . In our experiment, this ratio was more than 40 at 1.45  $\mu\text{m}$ . Thereby the deposition of Ag<sub>2</sub>S QDs on the surface of the Si leads to the formation of devices with a wider absorption band than that of the initial components separately.

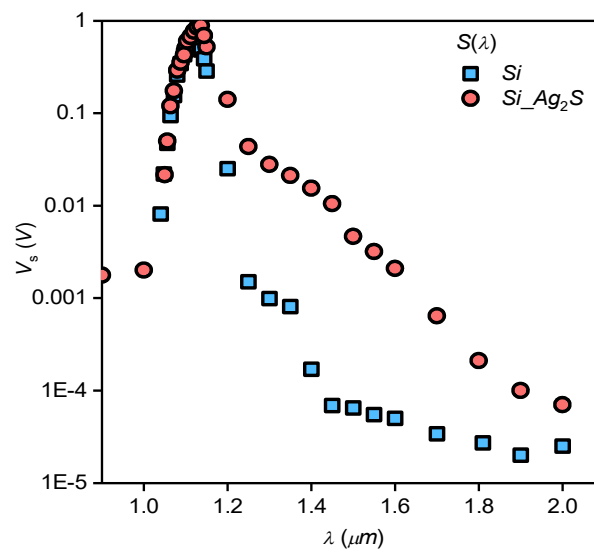


**Figure 2.** Spectral response  $S_v(\lambda)$  of Si and Si\_Ag<sub>2</sub>S devices. The curves reflect the effect of

Si sensitization caused by the absorption of a sub-band gap IR photon. The electron absorbed IR photon from valence band of Si transits at sub-band surface state  $\text{Ag}_2\text{S}$ . This process affects the space charge region near the Ti/Au contacts.

In order to clarify this phenomenon, a current-voltage (IV) curve of the  $\text{Si\_Ag}_2\text{S}$  device was investigated experimentally. **Figure 3a** shows experimental IV curves of the  $\text{Si\_Ag}_2\text{S}$  device illuminated by IR light of various power levels at  $1.55\ \mu\text{m}$ . As can be seen, at a low bias the IV curves of the device are not symmetric about zero. Referring to **Figure 3b**, the  $\text{Si\_Ag}_2\text{S}$  device utilizes two metal/semiconductor (MS) Ti/Si junctions. In the ideal case described by the Schottky-Mott theory, each such a junction is characterized by the appearance of a barrier in the vicinity of the MS interface caused by the difference of the metal's work function and the semiconductor's electron affinity. Given that Si possesses the interface behavior parameter of a small value, a space charge region and a built-in potential  $\phi_{bi}$  are formed at the interface which noticeably affects the transport of carriers through the junction near the Ti/Au contacts.<sup>[32]</sup>

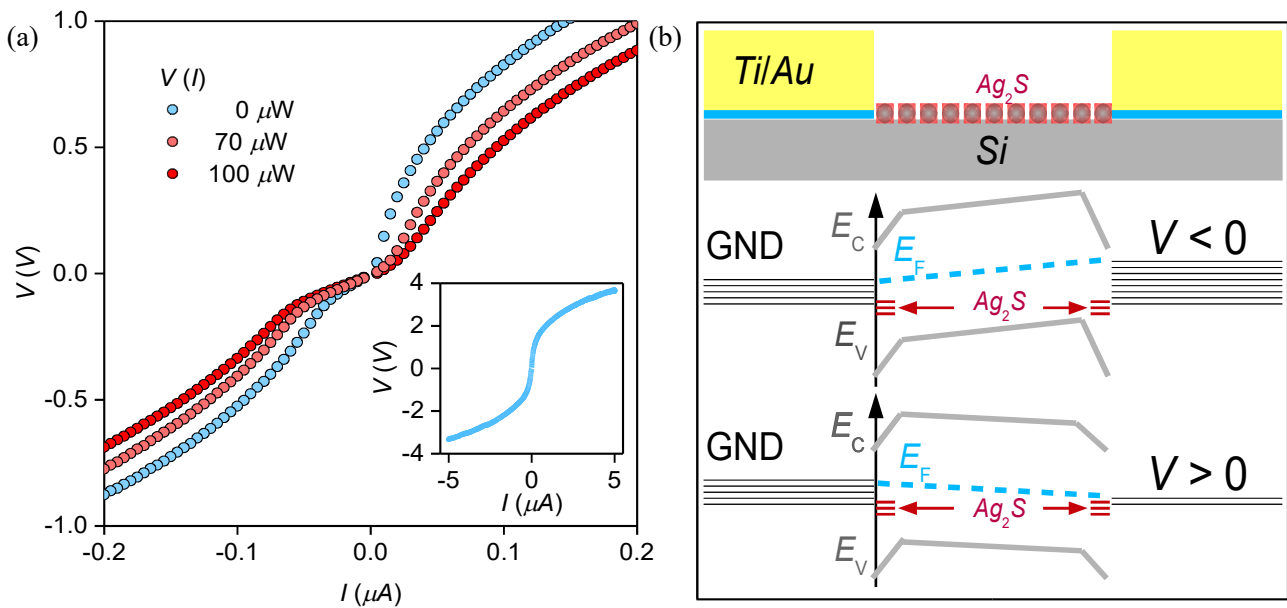


**Figure 3.** a) IV curves of a  $\text{Si\_Ag}_2\text{S}$  device under different IR power levels at  $1.55\ \mu\text{m}$ . The left insert presents an IV curve with no IR power for a wide bias range. The behavior of the IV

curve suggests the "hole" conductivity of the created Si<sub>2</sub>Ag<sub>2</sub>S devices and indicates large photoresponse. b) A schematic representation of the cross section of a Si<sub>2</sub>Ag<sub>2</sub>S device and its energy diagram (ED). In the vicinity of the Ti/Si junction a space charge region is formed due to the redistribution of electrons between Si and Ti. This fact is reflected on ED by the deformation of  $E_c$  and  $E_v$  band levels.

The sketch of the energy diagram presented in **Figure 3b** describes the behavior of the IV curve of the Si<sub>2</sub>Ag<sub>2</sub>S device in the case of positive and negative bias. When a positive potential is applied to the Ti/Au contact the IV curve displays a pronounced exponential character, as predicted by the thermionic emission model. The deviation from a truly exponential shape is caused by the variance of the Schottky contact area, which decreases in response to the increase of the forward bias voltage. Indeed, the contact area is proportional to the transfer length  $l_t = (\rho_c(V_j)/R_{sq})^{0.5}$  defined by the voltage-dependent contact resistivity of the Schottky contact ( $\rho_c$ ) and the sheet resistance of the Si wafer ( $R_{sq}$ ). Given that the Si<sub>2</sub>Ag<sub>2</sub>S device is essentially presented by two face-to-face connected Schottky diodes, an increase of the built-in potential ( $\phi_{bi}$ ) at the Si/Ti interface, at one end of the junction with a decrease of the  $\phi_{bi}$  at the other end is induced, when a negative potential is applied to it. In the case of small bias voltages, the IV curve is almost linear when a negative potential is applied to the Si/Ti interface. This behavior of the IV curve suggests the hole conductivity of the created Si<sub>2</sub>Ag<sub>2</sub>S devices. Thus the presence of a high response of the Si<sub>2</sub>Ag<sub>2</sub>S device above 1.25  $\mu\text{m}$  is explained by formation of impurity states in the band-gap of Si due to Ag<sub>2</sub>S QDs surface states. When an IR photon is absorbed by an electron in the Si valence band, the generated carrier transits at impurity state Ag<sub>2</sub>S in band-gap of the Si, this process owing to high carrier mobility in Si affects the built-in potential  $\phi_{bi}$  near the Ti/Au contacts.<sup>[33]</sup> The existence of the built-in potential  $\phi_{bi}$  near the Ti/Au contacts explains the zero bias mode of the devices.

Because of their non-stoichiometry, the Ag<sub>2</sub>S QDs have a high concentration of trap states. These trap states along with surface states in Si also could contribute to the Si<sub>2</sub>Ag<sub>2</sub>S detection

above 1.1  $\mu\text{m}$ . Since quantum dots do not come into contact with each other, the charge carriers from the  $\text{Ag}_2\text{S}$  trap states generated by the photoelectric effect and entering the Si increase its conductivity. The time constant of the Si- $\text{Ag}_2\text{S}$  detector will be determined by the characteristic lifetimes of the free charge carriers in the silicon/metal regions.

The noise equivalent power ( $NEP$ ) of the Si and Si- $\text{Ag}_2\text{S}$  devices was measured at 1.55  $\mu\text{m}$  in order of device quantity evaluation.

$$NEP = \frac{P}{V_s} \frac{V_n}{\sqrt{\Delta f}}, \frac{W}{\sqrt{\text{Hz}}}$$

A thermally stabilized laser diode at 1.55  $\mu\text{m}$  was used as a source. During measurements of the voltage responsivity, the laser diode power  $P$  was chosen so that the signal to noise ratio  $V_s/V_n$  did not exceed 1.5–2. This guaranteed the linear operation mode of the studied devices. The signal  $V_s$  and noise  $V_n$  voltages were measured at a modulation frequency of the IR radiation  $f$  of 80 Hz. The experimentally measured  $NEP$  for Si and Si- $\text{Ag}_2\text{S}$  structures were  $2.1 \cdot 10^{-8} \text{ W}/\sqrt{\text{Hz}}$  and  $4.5 \cdot 10^{-10} \text{ W}/\sqrt{\text{Hz}}$ , respectively. Given the Si IR range transparency and that the  $V_n$  behaves as  $1/f$  already at 10 KHz the estimated  $NEP$  for the Si- $\text{Ag}_2\text{S}$  device becomes of the order of  $10^{-13} \text{ W}/\sqrt{\text{Hz}}$ . The specific sensitivity of the Si- $\text{Ag}_2\text{S}$  device is of the order of  $10^{11} \text{ cm}/\sqrt{\text{HzW}^{-1}}$ , which is comparable with values of the best commercially available IR detectors.

In conclusion, this work presented a simple, low-cost and effective technology of extending the photoresponse of Si towards the IR range. The technology based on  $\text{Ag}_2\text{S}$  quantum dots allows creating controllable surface states in Si. At 1.45  $\mu\text{m}$  the response of the the Si- $\text{Ag}_2\text{S}$  detector exceeds that of a conventional Si detector by a factor of 40. The specific sensitivity of the Si- $\text{Ag}_2\text{S}$  device is of the order of  $10^{11} \text{ cm}/\sqrt{\text{HzW}^{-1}}$  at 1.55  $\mu\text{m}$ , which is comparable with values to the best commercially available IR detectors. Further development of this work towards the enhancement of the device sensitivity is concerned with optimizing the density of surface states in Si by using a mixture of quantum dots made from materials with different photoelectric thresholds of the internal photoelectric effect for the multi-color detection mode.



## Experimental Section

The aqueous synthesis of colloidal Ag<sub>2</sub>S QDs was based on the initial reagents of AgNO<sub>3</sub> and Na<sub>2</sub>S. In the first case, 0.262 g AgNO<sub>3</sub> and 0.276 g TGA dissolved in 50 ml of water were poured into a thermostatically controlled reactor at 25 °C containing 200 ml of water. Next, the pH in the reactor with dropping of 1M NaOH solution was adjusted to 10. After that, using a peristaltic pump, 50 ml of a solution containing 0.18 g of Na<sub>2</sub>S was infused into the reactor for 240 s. The solution in the reactor changed color from pale yellow to dark brown. To remove the reaction by-products, acetone was added to the 50% aqueous colloidal Ag<sub>2</sub>S QDs solution and centrifuged. In this case, QDs settled to the bottom of the tube, and the solution with undesirable components was removed. The resulting Ag<sub>2</sub>S QDs were redissolved in distilled water. The cleaning procedure was repeated several times.

The optical absorption spectra of the fabricated Ag<sub>2</sub>S QDs were investigated with a USB2000+ spectrophotometer with USB-DT emission source (Ocean Optics, USA). Photoluminescence spectra were obtained on the automated spectral complex based on the diffraction monochromator MDR-4. The highly stable low-noise photodiode PDF10C/M (ThorlabsInc., USA) with a built-in amplifier was used as a photodetector for the near-IR region. The laser diode LPC-836 (Mitsubishi, Japan) operating at 660 nm was used as a source of photoluminescence excitation. The position of the characteristic feature in optical absorbance is 1.88 eV. In the luminescence spectra of our Ag<sub>2</sub>S QDs, a wide band with a maximum at 950 nm is observed. The significant Stokes shift relative to the position of the exciton transition in the optical absorption spectra and the FWHM of the luminescence spectra indicate the recombination nature of the observed emission.

The Si surface cleaning process was performed in Corial 200R, sequentially ion etching in O<sub>2</sub> for 15 s at 50 W and ion etching in Ar for 20 s at 50 W. Liquid etching with hydrofluoric acid (HF:H<sub>2</sub>O=1:10) took 30 s. The contacts to the Si structure were formed by thermal deposition of Ti and Au to thicknesses of 5 nm and 200 nm respectively. Ag<sub>2</sub>S QDs were deposited on top of the cleaned surface of a Si wafer by centrifuging for 1 min at 2000 rpm and heating to 120 °C on

hotplate.

Structural properties of the centrifuged Ag<sub>2</sub>S QDs were studied with the standard techniques of TEM and XRD analysis. The sizes of the synthesized ensembles of colloidal Ag<sub>2</sub>S QDs were determined with the TEM Carl Zeiss Libra 120 operating at 120 kV. High resolution TEM images were obtained with a JEOL HRes Carl Zeiss Libra microscope 200 kV. The crystal structure was investigated with the X-ray diffractometer ARL X'TRA for K<sub>α1</sub> of copper.

Optical spectral and NEP measurements were performed with the infrared spectrometer with a Xe lamp as a IR radiation source and the laser diod TeraXion PS-LM-1550.12-40-06 (from PureSpectrum). Precise attenuation and measurement of the IR power was done with the tunable attenuator EXFO FVA-600 and OPHIR VEGA ROHS respectively. A hyper-hemispherical Si lens ( $\rho > 10 \text{ K}\Omega \cdot \text{cm}$ ) with a diameter of 12 mm and an extension for wafer with a thickness of 350  $\mu\text{m}$  was used for the coupling the device with IR radiation. The IV curves of the device were measured by Keithley 2410. The signal and noise voltage within spectral and NEP measurements were measured by the Lock-in Amplifiers SR830 and UNIPAN 233 .

## Acknowledgements

The study of the spectral response and the fabrication of the devices were made with the support of the Russian Science Foundation (project No. 17-72-30036), the study of the NEP and the responsivity was carried out with the support of the Ministry of Education and Science of the Russian Federation [State Task number 11.2423.2017/4.6].

## References

- [1] International Technology Roadmap for Semiconductors, [www.itrs2.net](http://www.itrs2.net), **2016**.
- [2] Schwierz, F., Wong, H. & Liou, J. J. *Nanometer CMOS*, Pan Stanford, **2010**.
- [3] Soref, R. *Nat. Photon*, **2015**, 9, 358–359.
- [4] Ackert, J. J. et al. High-speed detection at two micrometres with monolithic silicon photodiodes. *Nat. Photon*, **2015**, 9, 393–396.

- [5] J. P. Mailoa, A. J. Akey, C. B. Simmons, D. Hutchinson, J. Mathews, J. T. Sullivan, D. Recht, M. T. Winkler, J. S. Williams, J. M. Warrender, P. D. Persans, M. J. Aziz, T. Buonassisi, *Nat. Commun.* **2014**, 5, 3011.
- [6] Xiaoping Liu, Bart Kuyken, Gunther Roelkens, Roel Baets, Richard M. Osgood Jr & William M. J. Green, *Nat. Photon.* **2012**, 6, 667–671.
- [7] Yonder Berencén, Slawomir Prucnal, Fang Liu, Ilona Skorupa, René Hübner, Lars Rebohle, Shengqiang Zhou, Harald Schneider, Manfred Helm & Wolfgang Skorupa, *Sci. Rep.* **2017**, 7, 43688.
- [8] Xiaodong Qiu, Xuegong Yu, Shuai Yuan, Yuhan Gao, Xuemei Liu, Yang Xu, Deren Yang, *Adv. Opt. Mater.* **2018**, 6, 1700638.
- [9] E. Pérez, H. Castán, H. García, S. Dueñas, L. Bailón, D. Montero, R. García-Hernansanz, E. García-Hemme, J. Olea, and G. González-Díaz, *Appl. Phys. Lett.* **2015**, 106, 022105.
- [10] Jonathan P. Mailoa, Austin J. Akey, Christie B. Simmons, David Hutchinson, Jay Mathews, Joseph T. Sullivan, Daniel Recht, Mark T. Winkler, James S. Williams, Jeffrey M. Warrender, Peter D. Persans, Michael J. Aziz & Tonio Buonassisi, *Nat. Commun.* **2014**, 5, 3011.
- [11] Simmons, Christie B., Austin J. Akey, Jonathan P. Mailoa, Daniel Recht, Michael J. Aziz, and Tonio Buonassisi, *Adv. Funct. Mater.* **2014**, 24, 2852.
- [12] Hyun Wook Shin, Sang Jun Lee, Doo Gun Kim, Myung-Ho Bae, Jaeyeong Heo, Kyoung Jin Choi, Won Jun Choi, Jeong-woo Choe & Jae Cheol Shin, *Sci. Rep.* **2016**, 5, 10764.
- [13] Han, S.-J., Garcia, A. V., Oida, S., Jenkins, K. A. & Haensch, W., *Nat. Commun.* **2014**, 5, 3086.
- [14] Andreas Pospischil, Markus Humer, Marco M. Furchi, Dominic Bachmann, Romain Guider, Thomas Fromherz & Thomas Mueller, *Nat. Photon.* **2013**, 7, 892–896.
- [15] Xuetao Gan, Ren-Jye Shiue, Yuanda Gao, Inanc Meric, Tony F. Heinz, Kenneth Shepard, James Hone, Solomon Assefa & Dirk Englund, *Nat. Photon.* **2013**, 7, 883–887.
- [16] Wang, X., Cheng, Z., Xu, K., Tsang, H. K. & Xu, J., *Nat. Photon.* **2013**, 7, 888–891.
- [17] Stijn Goossens, Gabriele Navickaite, Carles Monasterio, Shuchi Gupta, Juan José Piqueras,

Raúl Pérez, Gregory Burwell, Ivan Nikitskiy, Tania Lasanta, Teresa Galán, Eric Puma, Alba Centeno, Amaia Pesquera, Amaia Zurutuza, Gerasimos Konstantatos & Frank Koppens, *Nat. Photon.* **2017**, 11, 366-371

[18] S. Schmitt-Pink, D.A.B. Miller, D.C. Chemla, *Phys. Rev. B.* **1987**. 35, 1, 8113-8125.

[19] Gerasimos Konstantatos, Michela Badioli, Louis Gaudreau, Johann Osmond, Maria Bernechea, F. Pelayo Garcia de Arquer, Fabio Gatti & Frank H. L. Koppens, *Nat. Nano.* **2012**, 7, 363-368.

[20] Zhenhua Sun, Zhike Liu, Jinhua Li, Guo-an Tai, Shu-Ping Lau, Feng Yan, *Adv. Mater.* **2012**, 24, 5878.

[21] Wenhao Guo, Shuigang Xu, Zefei Wu, Ning Wang, M. M. T. Loy, Shengwang Du, *Small* **2013**, 9, 3031.

[22] Steven A. McDonald, Gerasimos Konstantatos, Shiguo Zhang, Paul W. Cyr, Ethan J. D. Klem, Larissa Levina & Edward H., Sargent. *Nat. Mater.* **2005**, 4, 138.

[23] Guanghui Su, Chao Liu, Zhao Deng, Xiujian Zhao, and Xuedong Zhou, *Opt. mater. exp.* **2017**, 7, 7, 2194-2207.

[24] A.L. Efros & D.J. Nesbitt, *Nat. nano.* **2016**, 11, 661-671.

[25] Rui Tang, Jianpeng Xue, Baogang Xu, Duanwen Shen, Gail P. Sudlow and Samuel Achilefu, *ACS Nano.* **2015**, 9, 1, 220-230.

[26] A. N. Rodr'iguez, M. T. S. Nair, P. K. Nair, *Semicond. Sci. Technol.* **2005**, 20, 576.

[27] S. Lin, Y. Feng, X. Wen, P. Zhang, S. Woo, S. Shrestha, G. Conibeer, S. Huang, *J. Phys. Chem. C.* **2015**, 119, 867–872.

[28] S.I. Sadovnikov, A.I. Gusev, A.A. Rempel, *Rev. Adv. Mater. Sci.* **2015**, 41, 7-19.

29. S. I. Sadovnikov, A. I. Gusev, E. Yu. Gerasimov, A. A. Rempel, *Chem. Phys. Lett.* **2015**, 642, 17-21.

[30] O. V. Ovchinnikov, M. S. Smirnov, T. S. Kondratenko, A. S. Perepelitsa, I. G. Grevtseva, S. V. Aslanov, *Optics and spectroscopy* **2018**, 125, 1, 107-112.

[31] M.S. Smirnov, O.V. Ovchinnikov, I.G. Grevtseva, A.I. Zvyagin, A.S. Perepelitsa, R.A. Ganeev,

*Optics and Spectroscopy* **2018**, 124, 5, 681-686.

[32] Raymond T. Tung, *Applied Physics Reviews* **2014**, 1, 011304.

[33] Prince M.B. *Phys. Rev.* **1953**, 92, 681.